exchange with polysulfates (Fig. 3C). It is also worth mentioning that the elimination of Chol-siRNA micelles from the bloodstream followed a single exponential decay (or a one-compartment model in pharmacokinetics) (Fig. S8B), suggesting that the Chol-siRNA micelles were eliminated mainly from the kidney without being distributed into peripheral tissues. This is supported by the result that the Chol-siRNA micelles (or the siRNA payloads) were mainly accumulated in the kidney after systemic administration (Fig. S9). Note that the blood retention time of naked Chol-siRNA was modestly longer than those of naked Chol-free siRNA. This may be due to interaction of Chol-siRNA with lipoproteins in the bloodstream leading to compromised renal filtration [39].

Next, the tumor-targeting ability of cRGD-installed micelles was investigated by measuring their accumulation in subcutaneous HeLa-Luc tumors. Fluorescently-labeled micelles were administered by tail vein injection and tumors were excised after 4 h followed by measurement of the fluorescence intensity of each tumor mass with an IVIS instrument. While there was almost no difference in fluorescence intensity between Chol-free micelles with and without cRGD, significantly higher fluorescence intensity was observed for Chol-siRNA micelles equipped with cRGD, compared to those without cRGD (Fig. 5B). These results indicate that the cRGD ligand enabled more efficient tumor accumulation of the highly stabilized Chol-siRNA micelles following systemic administration, presumably due to the enhanced avidity of cRGD ligands to $\alpha_v\beta_3/\alpha_v\beta_5$ integrin receptors on cancerous cells and also tumor-associated endothelial cells [13,33,34]. Intratumoral distribution of RGD(+)/Chol(+) micelles was further examined by continuous CLSM observation of the subcutaneous tumor tissue after systemic administration. The CLSM image captured at 80 min after injection displays massive distribution of the micelles in the tumor tissue through the blood vessels (Fig. S10). Importantly, there were no significant differences in healthy organ/tissue accumulation between non-targeted and actively-targeted micelles ($p > 0.05$) (Fig. S9), demonstrating tumor-selective targeting of RGD(+)/Chol(+) micelles.

Finally, the *in vivo* gene silencing activity of siRNA micelles was investigated through luciferase gene silencing (luminescence measurement) in subcutaneous HeLa-Luc tumors, similar to the luminescence-based assay used for *in vitro* experiments. At 48 h after the initial injection of samples (total 3 intravenous injections), luciferin solution was intraperitoneally injected into mice, followed by measurement of the luminescence intensity in the tumor tissues with an IVIS instrument (Fig. 5C and Fig. S11). Non-targeted RGD(−)/Chol(−) micelles did not decrease tumor luminescence intensity, whereas the actively-targeted, RGD(+)/Chol(−) and RGD(+)/Chol(+) micelles did reduce tumor luminescence intensities compared to buffer-treated controls. In particular, the actively-targeted/stabilized, RGD(+)/Chol(+) micelles achieved significant decrease in the luminescence intensity ($p < 0.05$ for buffer-treated controls). It should be noted that the RGD(+)/Chol(+) micelles carrying siScr as a control sequence caused no decrease in the luminescence intensity, demonstrating sequence-specific gene silencing (i.e. RNAi) activity of the actively-targeted/stabilized micelles. In addition, it was also confirmed that all the tested micelles did not induce significant changes in the body weight of tumor-bearing mice (Table S1). In total, actively-targeted and stabilized micelles were more effective in delivering intact (thus active) siRNA to the cytoplasm of tumor cells following systemic administration. The present study particularly focused on the separate functionalization of the macromolecular components, i.e., PEG-PLL and siRNA, for construction of the multifunctional formulation, i.e., actively-targeted/stabilized micelles. This approach permitted the facile functionalization based on a simple chemistry, which is in contrast to the previously developed block copolymer modified with 2-iminothiolane, where two functional groups, open chain and closed ring structures, are equilibrated in the side chain of PLL [13].

4. Conclusions

Actively-targeted and stabilized PIC micelles were constructed with Chol-siRNA and PEG-PLL comprising the cRGD ligand at the PEG terminus and thiol (and amidine) functionality in PLL side chains, for systemic siRNA delivery to solid tumors. The Chol modification of siRNA allowed the production of PIC micelles at wider mixing ratios above the charge-stoichiometric point and dramatically stabilized the micelle structure, resulting in the enhanced blood circulation property of siRNA micelles. Further, the active targeting ability of the cRGD ligand was proven by enhanced cellular uptake *in vitro* and also enhanced tumor accumulation *in vivo* following systemic administration. Ultimately, the synergistic effect of active targetability and improved stability enabled significant sequence-specific gene silencing in the subcutaneous tumor tissue following systemic administration of siRNA micelles. The results obtained in this study highlight the importance of additional stabilizing mechanisms in PIC micelle systems, and that stabilization can be achieved from both the polymer component and the siRNA component used. Here, Chol-conjugation to siRNA reinforced the limited effect of disulfide cross-linking, thus improving the active targetability of nanoparticulate formulations for systemic transport of siRNA into tumor tissues.

Acknowledgments

This research was financially supported by the Funding Program for World-Leading Innovate R&D in Science and Technology (FIRST) (JSPS), Grants-in-Aid for Scientific Research of MEXT (JSPS KAKENHI Grant Numbers 25000006 and 25282141), the Center of Innovation (COI) Program (JST), Grants-in-Aid for Scientific Research of MHLW, National Institute of Biomedical Innovation and Mochida Memorial Foundation for Medical and Pharmaceutical Research.

Appendix A. Supplementary data

Supplementary data related to this article can be found online at http://dx.doi.org/10.1016/j.biomaterials.2014.05.041.

References

[1] Fire A, Xu S, Montogomery M, Kostas S, Driver S, Mello C. Potent and specific genetic interference by double stranded RNA in caenorhabditis elegans. Nature 1998;391:806–11.
[2] Elbashir SM, Harborth J, Lendeckel W, Yalcin A, Weber K, Tuschl T. Duplexes of 21-nucleotide RNAs mediate RNA interference in cultured mammalian cells. Nature 2001;411:494–8.
[3] Burnett JC, Rossi JJ. RNA-based therapeutics: current progress and future prospects. Chem Biol Rev 2012;19:60–71.
[4] Carthew R, Sontheimer E. Origins and mechanisms of miRNA and siRNAs. Cell 2009;136:642–55.
[5] Turner J, Jones S, Moschos S, Lindsay M, Gait M. MALDI-TOF mass spectral analysis of siRNA degradation in serum confirms an RNase A-like activity. Mol Biosyst 2007;3:43–50.
[6] Van de Water F, Boerman O, Wouterse A, Peters J, Russel F, Masereeuw R. Intravenously administered short interfering RNA accumulates in the kidney and selectively suppresses gene function in renal proximal tubules. Drug Metab Dispos 2006;34:1393–7.
[7] Schiffelers RM, Ansari A, Xu J, Zhou Q, Tang Q, Strom G, et al. Cancer siRNA therapy by tumor selective delivery with ligand-targeted sterically stabilized nanoparticle. Nucleic Acids Res 2004;32:e149.
[8] Song E, Zhu P, Lee SK, Chowdhury D, Kussman S, Dykxhoorn DM, et al. Antibody mediated in vivo delivery of small interfering RNAs via cell-surface receptors. Nat Biotechnol 2005;23:709–17.

[9] McNamara II JO, Andrechek ER, Wang Y, Viles KD, Rempel RE, Gilboa E, et al. Cell type-specific delivery of siRNAs with aptamer-siRNA chimeras. Nat Biotechnol 2006;24:1005–15.
[10] Li SD, Chen YC, Hackett MJ, Huang L. Tumor-targeted delivery of siRNA by self-assembled nanoparticles. Mol Ther 2008;16:163–9.
[11] Wang XL, Xu R, Wu X, Gillespie D, Jensen R, Lu ZR. Targeted systemic delivery of a therapeutic siRNA with a multifunctional carrier controls tumor proliferation in mice. Mol Pharm 2009;6:738–46.
[12] Davis ME, Zuckerman JE, Choi CHJ, Seligson D, Tolcher A, Alabi CA, et al. Evidence of RNAi in humans from systemically administered siRNA via targeted nanoparticles. Nature 2010;64:1067–70.
[13] Christie RJ, Matsumoto Y, Miyata K, Nomoto T, Fukushima S, Osada K, et al. Targeted polymeric micelles for siRNA treatment of experimental cancer by intravenous injection. ACS Nano 2012;6:5174–89.
[14] Dohmen C, Edinger D, Frohlich T, Schreiner L, Lachelt U, Troiber C, et al. Nanosized multifunctional polyplexes for receptor-mediated siRNA delivery. ACS Nano 2012;26:5198–208.
[15] Lee H, Lytton-Jean AKR, Chen Y, Love KT, Park AI, Karagiannis ED, et al. Molecularly self-assembled nucleic acid nanoparticles for targeted in vivo siRNA delivery. Nat Nanotechnol 2012;7:389–93.
[16] Kim HJ, Ishii T, Zheng M, Watanabe S, Toh K, Matsumoto Y, et al. Multifunctional polyion complex micelle featuring enhanced stability, targetability, and endosome escapability for systemic siRNA delivery to subcutaneous model of lung cancer. Drug Deliv Transl Res 2014;4:50–60.
[17] Jule E, Nagasaki Y, Kataoka K. Surface plasmon resonance study on the interaction between lactose-installed poly(ethylene glycol)-poly(D, L-lactide) block copolymer micelles and lectins immobilized on a gold surface. Langmuir 2002;18:10334–9.
[18] Alam MR, Ming X, Fisher M, Lackey JG, Rajeev KG, Manoharan M, et al. Multivalent cyclic RGD conjugates for targeted delivery of small interfering RNA. Bioconjug Chem 2011;22:1673–81.
[19] Harada A, Kataoka K. Formation of polyion complex micelles in an aqueous milieu from a pair of oppositely-charged block copolymers with poly(ethylene glycol) segments. Macromolecules 1995;28:5294–9.
[20] Kataoka K, Togawa H, Harada A, Yasugi K, Matsumoto T, Katayose S. Spontaneous formation of polyion complex micelles with narrow distribution from antisense oligonucleotide and cationic block copolymer in physiological saline. Macromolecules 1996;29:8556–7.
[21] Kakizawa Y, Kataoka K. Block copolymer micelles for delivery of gene and related compounds. Adv Drug Deliv Rev 2002;54:203–22.
[22] Miyata K, Nishiyama N, Kataoka K. Rational design of smart supramolecular assemblies for gene delivery: chemical challenges in the creation of artificial viruses. Chem Soc Rev 2012;41:2562–74.
[23] Kim HJ, Oba M, Pittella F, Nomoto T, Cabral H, Matsumoto Y, et al. PEG-detachable cationic polyaspartamide derivatives bearing stearoyl moieties for systemic siRNA delivery toward subcutaneous BxPC3 pancreatic tumor. J Drug Target 2012;20:33–42.
[24] Kakizawa Y, Harada A, Kataoka K. Environment-sensitive stabilization of core-shell structured polyion complex micelle by reversible cross-linking of the core through disulfide bond. J Am Chem Soc 1999;121:11247–8.
[25] Matsumoto S, Christie RJ, Nishiyama N, Miyata K, Ishii A, Oba M, et al. Environment-responsive block copolymer micelles with a disulfide cross-linked core for enhanced siRNA delivery. Biomacromolecules 2009;10:119–27.
[26] Christie RJ, Miyata K, Matsumoto Y, Nomoto T, Menasco D, Lai TC, et al. Effect of polymer structure on micelles formed between siRNA and cationic block copolymer comprising thiols and amidines. Biomacromolecules 2011;12:3174–85.
[27] Meister A, Anderson ME. Glutathione. Annu Rev Biochem 1983;52:711–60.
[28] Saito G, Swanson JA, Lee KD. Drug delivery strategy utilizing conjugation via reversible disulfide linkages: role and site of cellular reducing activities. Adv Drug Deliv Rev 2013;55:199–215.
[29] Soutschek J, Akinc A, Bramlage B, Charisse K, Constien R, Donoghue M, et al. Therapeutic silencing of an endogenous gene by systemic administration of modified siRNAs. Nature 2004;432:173–8.
[30] Oba M, Miyata K, Osada K, Christie RJ, Sanjoh M, Li W, et al. Polyplex micelles prepared from ω-cholesteryl PEG-polycation block copolymers for systemic gene delivery. Biomaterials 2011;32:652–63.
[31] Oba M, Fukushima S, Kanayama N, Aoyagi K, Nishiyama N, Koyama H, et al. Cyclic RGD peptide-conjugated polyplex micelles as a targetable gene delivery system directed to cells possessing αvβ3 and αvβ5 integrins. Bioconjug Chem 2007;18:1415–23.
[32] Matsumoto Y, Nomoto T, Cabral H, Mastumoto Y, Watanabe S, Christie RJ, et al. Direct and instantaneous observation of intravenously injected substances using intravital confocal micro-videography. Biomed Opt Express 2010;1:1209–16.
[33] Ruoslahti E. RGD and recognition sequences for integrins. Annu Rev Cell Dev Biol 1996;12:697–715.
[34] Xiong J, Stehle T, Zhang R, Joachimiak A, Frech M, Goodman S, et al. Crystal structure of the extra-cellular segment of integrin αvβ3 in complex with an Arg-Gly-Asp ligand. Science 2002;296:151–5.
[35] Itaka K, Yamauchi K, Harada A, Nakamura K, Kawaguchi H, Kataoka K. Polyion complex micelles from plasmid DNA and poly(ethyleneglycol)-poly(L-lysine) block copolymer as serum-tolerable polyplex system: physicochemical properties of micelles relevant to gene transfection efficiency. Biomaterials 2003;24:4495–506.
[36] Zukerman JE, Choi CHJ, Han H, Davis ME. Polycation-siRNA nanoparticles can disassemble at the kidney glomerular basement membrane. Proc Natl Acad Sci U S A 2012;109:3137–42.
[37] Shayakhmetov DM, Eberly AM, Li ZY, Lieber A. Deletion of penton RGD motifs affects the efficiency of both the internalization and the endosome escape of viral particles containing adenovirus serotype 5 or 35 fiber knobs. J Virol 2005;79:1053–61.
[38] Symonds P, Murray JC, Hunter AC, Debska G, Szewczyk A, Moghimi SM. Low and high molecular weight poly(L-lysine)s/poly(L-lysine)-DNA complexes initiate mitochondrial-mediated apoptosis differently. FEBS Lett 2005;579:6191–8.
[39] Wolfrum C, Shi S, Jayaprakash KN, Jayaraman M, Wang G, Pandey RK, et al. Mechanisms and optimization of *in vivo* delivery of lipophilic siRNAs. Nat Biotechnol 2007;25:1149–57.

Virchows Arch (2015) 466:265–277
DOI 10.1007/s00428-014-1705-4

ORIGINAL ARTICLE

An immunohistochemical marker panel including claudin-18, maspin, and p53 improves diagnostic accuracy of bile duct neoplasms in surgical and presurgical biopsy specimens

Yoshiko Keira · Akira Takasawa · Masaki Murata · Masanori Nojima · Kumi Takasawa · Jiro Ogino · Yukimura Higashiura · Ayaka Sasaki · Yasutoshi Kimura · Toru Mizuguchi · Satoshi Tanaka · Koichi Hirata · Norimasa Sawada · Tadashi Hasegawa

Received: 1 July 2014 / Revised: 6 October 2014 / Accepted: 2 December 2014 / Published online: 14 December 2014

Abstract Biliary tract cancers have an extremely poor outcome, and specific diagnostic markers and effective treatments are needed urgently. In this study, we assessed the capacity of panel of immunohistochemical markers including claudin-18, maspin, and p53 to distinguish biliary tract carcinoma and biliary intraepithelial neoplasia (BilIN) from non-neoplastic epithelium. We performed a retrospective study of 66 biliary tract cancer specimens and 63 specimens with non-neoplastic lesions. Of the surgical specimens, 96.7 % with adenocarcinoma/BilIN were detected as neoplastic, and all 63 specimens histologically diagnosed as non-neoplastic lesion were detected as non-neoplastic with high sensitivity (91.1 %) and specificity (100 %). Of presurgical endobiliary forceps biopsy specimens, all with adenocarcinoma/BilIN and only 1 of the 19 with a non-neoplastic lesion were distinguished as neoplastic with high sensitivity (100 %) and specificity (94.7 %). Moreover, this panel provided good separation of neoplasm from malignancy-undetermined atypical epithelium (18/21, 85.7 %). This panel achieves a more reliable distinction of biliary tract cancers and BilINs from non-neoplastic epithelia in both surgical and biopsy specimens than immunohistochemical analysis with single antibodies and is useful in supporting a diagnosis of adenocarcinoma and BilIN.

Keywords Claudin-18 · Maspin · p53 · Human bile duct cancer · Early diagnosis

Electronic supplementary material The online version of this article (doi:10.1007/s00428-014-1705-4) contains supplementary material, which is available to authorized users.

Y. Keira · J. Ogino · T. Hasegawa
Departments of Surgical Pathology, Sapporo Medical University School of Medicine, Sapporo, Japan

A. Takasawa (✉) · M. Murata · K. Takasawa · Y. Higashiura · A. Sasaki · S. Tanaka · N. Sawada
Departments of Pathology, Sapporo Medical University School of Medicine, Sapporo, Japan
e-mail: atakasawa@sapmed.ac.jp

M. Nojima
Division of Advanced Medicine Promotion, The Advanced Clinical Research Center, The Institute of Medical Science, The University of Tokyo, Tokyo, Japan

Y. Kimura · T. Mizuguchi · K. Hirata
Departments of Surgery, Surgical Oncology, and Science, Sapporo Medical University School of Medicine, Sapporo, Japan

Introduction

The incidence of biliary tract cancers, comprising gallbladder, bile duct, and ampullary cancer, has been increasing worldwide over the past several decades and in the USA over the last decade [1, 2]. In Japan, the morbidity associated with these cancers has also increased, and more than 18,000 people died of this cancer in 2012 [3].

Generally, the overall prognosis for biliary tract cancer is poor. Although currently only surgical resection may be curative, the curative resection rate has remained low at approximately 40 % [4]. Therefore, early detection and preoperative confirmation of the malignant diagnosis is vitally important in improving prognosis [5]. The gold standard method of diagnosis requires endobiliary forceps biopsy and percutaneous liver biopsy. However, histopathological examination of biopsy tissues in clinical practice can be challenging because of a limited amount of material, crush artifacts, and the presence of confounding acute and chronic inflammatory epithelial changes [6, 7].

The need for accurate diagnostic methods has led to the exploration of immunohistochemical markers to distinguish

between benign atypia and malignancy [8–13]. In the present study, we examined the potential of three molecules, claudin-18 (cldn18), maspin, and p53, to serve as immunohistological diagnostic markers for bile duct cancers, biliary intraepithelial neoplasia (BilIN), and ampullary cancer, which can be difficult to diagnose by histology alone. BilIN is a flat-type premalignant or in situ neoplastic lesion of the biliary tract that was first documented in 2005 and has been recently included in the WHO classification of 2010 as intraductal papillary neoplasm of the bile duct (IPNB) [14–16]. BilIN occurs in intrahepatic and extrahepatic bile ducts and sometimes result from disorders of the biliary tract, such as hepatolithiasis, choledochal cysts, and primary sclerosing cholangitis. Biliary tract cancers progress through multistep carcinogenesis, with multiple molecular events such as KRAS and GNAS mutation and p53 overexpression, and BilIN and IPN are precursor lesions [15, 17]. BilIN is subdivided into BilIN-1, BilIN-2, and BilIN-3 according to the degree of cellular atypia and architectural disturbance. BilIN-1 and BilIN-2 correspond to low and intermediate grades, respectively. BilIN-3 is high grade and equivalent to carcinoma in situ.

Claudins are tight junction resident transmembrane proteins that are present in epithelial and endothelial cells and in derived neoplastic cells [18]. Aberrant expression of a number of claudins has been reported in various carcinomas [19, 20]. Cldn18 is detected in gastrointestinal and lung tissues [21–23]. In pancreatic ductal adenocarcinoma, cldn18 is overexpressed and has been identified as a potential diagnostic marker [24]. In the biliary tract, multivariable analysis demonstrated that positive cldn18 expression is an independent risk factor for lymph node metastasis [25]. Recently, we reported that cldn18 is primarily regulated at the transcriptional level via specific protein kinase C signaling pathways and that its expression is modified by DNA methylation [26].

Mammary serine protease inhibitor, otherwise known as maspin, is a member of the serine protease inhibitor superfamily and was identified as a tumor suppressor in mammary tissue in 1994 [27]. However, subsequent studies have revealed its tumor-suppressive properties to be complex and dependent on factors such as genetic background, type of cancer, and the expression of maspin (or lack thereof) in the corresponding normal tissue. Interestingly, both methylation and demethylation of the *maspin* promoter have been reported to influence its expression [28]. Some studies demonstrated an association between hypermethylation of the *maspin* promoter and loss of maspin expression in colonic and ovarian cancers [29, 30]. Others reported that demethylation was associated with maspin overexpression in gastric cancer [31]. In biliary tract cancer, demethylation of the *maspin* promoter and aberrant maspin expression has been reported [32]. In pancreatic ductal adenocarcinoma, overexpression of maspin is associated with lower postoperative survival [33]. In the gallbladder, use of an immunohistochemical panel including maspin has been reported to distinguish adenocarcinoma from benign/reactive epithelium [34].

Mutation of the *p53* gene is a key event in the carcinogenesis of many different types of tumors. The presence of this genetic abnormality in biliary tract cancer has been suggested in various investigations that used immunohistochemical and molecular epidemiological methods [35, 36].

Currently, accurate cancer detection including localization is needed to improve the prognosis of patients with bile duct cancers. In this study, we used immunohistochemical methods to document the expression of cldn18, maspin, and p53 in bile duct carcinomas, BilINs, and ampullary carcinoma in surgical specimens and analyzed the diagnostic utility of this immunohistochemical panel in presurgical bile duct biopsy specimens.

Materials and methods

Surgical specimens

A total of 66 biliary tract cancer specimens obtained by surgical excision from 1999 to 2011 were retrieved from the pathology file of Sapporo Medical University Hospital, Sapporo, Japan. Their clinicopathological characteristics are summarized in Table 1. Gallbladder cancer was excluded from the present study because presurgical biopsies had not been performed. The histological type of all cancers was adenocarcinoma. The cancer staging system was based on both the UICC classification (7th edition) and the Japanese Society of Biliary Surgery classification (fifth edition). Among the 66 adenocarcinomas, 25 (9 intrahepatic, 5 hilar extrahepatic bile duct, 7 distal extrahepatic bile duct, and 4 ampulla of Vater) had flat intraepithelial neoplastic lesions around invasive carcinomas. These intraepithelial lesions consisted of precursor lesions, that is, true BilIN, and superficial spreading lesions that were difficult to differentiate. Thus, in the present study, all intraepithelial components were classified as BilIN-1, BilIN-2, and BilIN-3 according to the degree of cell atypia. In addition, 63 specimens with non-neoplastic epithelia from cases of adenocarcinoma (25 intrahepatic, 10 hilar extrahepatic bile duct, 21 distal extrahepatic bile duct, and 7 ampulla of Vater) were selected as a control group. All slides were independently evaluated by three pathologists (KY, TA, and MM). Discordant cases were discussed, and a consensus was reached.

Immunohistochemical staining of surgical specimens

The hematoxylin and eosin (H&E)-stained slides from all cases were reviewed to select representative sections. New sections from paraffin blocks were examined by the labeled polymer method. Sections were deparaffinized, rehydrated, moistened with phosphate-buffered saline (PBS; pH 7.4),

Table 1 Clinicopathological features of biliary tract cancers

Total (N=66)		Intrahepatic bile duct carcinoma (N=27)		Extrahepatic bile duct carcinoma (N=32)		Ampullary carcinoma (N=7)	
Age (range, median)	39–84, 68.5	T grade (UICC)		T grade (UICC)		T grade (UICC)	
Sex		T1/T2	22	Tis/T1/T2	18	Tis/T1/T2	4
Male	47	T3/T4	5	T3/T4	14	T3/T4	3
Female	19	T grade[b]		T grade[b]		T grade[b]	
Location		T1/T2	14	T1/T2	11	T1/T2	2
Intrahepatic	27	T3/T4	13	T3/T4	21	T3/T4	5
Extrahepatic	32	Lymph node metastasis		Lymph node metastasis		Lymph node metastasis	
Hilar	11	Negative	24	Negative	20	Negative	4
Distal	21	Positive	3	Positive	12	Positive	3
Ampulla of Vater	7	Stage group (UICC)		Stage group (UICC)		Stage group (UICC)	
Tumor size		I/II	20	0/IA/IB/II	15	0/IA/IB/II	2
≦3 cm	29	III/IV	7	IIA/IIB/IIIA/IIIB	17	IIA/IIB/IIIA/IIIB	5
>3 cm	25	Stage group[b]		Stage group[b]		Stage group[b]	
Unknown	12	I/II	13	I/II/III	17	I/II/III	3
Histological type		III/IVA/IVB	14	IVA/IVB	15	IVA/IVB	4
Well	33	Lymphatic invasion		Lymphatic invasion		Lymphatic invasion	
Moderately	16	Negative	–	Negative	13	Negative	2
Poorly	17	Positive	–	Positive	19	Positive	5
BilIN[a]		Venous invasion		Venous invasion		Venous invasion	
BilIN-1	8	Negative	18	Negative	16	Negative	3
BilIN-2	11	Positive	9	Positive	23	Positive	4
BilIN-3	6			Interstitial connective tissue		Interstitial connective tissue	
				Medullary	4	Medullary	1
				Intermediate	20	Intermediate	6
				Scirrhous	8	Scirrhous	0

[a] Flat intraepithelial neoplastic lesion around invasive carcinoma classified as BilIN-1, BilIN-2, and BilIN-3 according to the degree of cell atypia

[b] General rules for surgical and pathological studies on cancer of the biliary tract (fifth edition) by the Japanese Society of Biliary Surgery

and then pretreated in an autoclave at 121 °C for 5 min in 10 mM citrate buffer (pH 6.0), followed by 30 min incubation with antibodies to the following antigens in an automated immunostaining system (Dako Autostainer; Dako, Carpinteria, CA, USA): cldn18 (Invitrogen, Carlsbad, CA; polyclonal, ×100), maspin (BD, Franklin Lakes, NJ; G167-70, ×50), and p53 (Dako, DO-7, ×50). Maspin immunoreactivity was independently evaluated in the cytoplasm (C) or nucleus (N). The intensity of staining was assessed as strong (3), moderate (2), weak (1), or negative (0). The proportion of neoplastic cells stained was recorded as 0 (no staining), 1 (1–10 %), 2 (11–20 %), 3 (21–30 %), 4 (31–40 %), 5 (41–50 %), 6 (51–60 %), 7 (61–70 %), 8 (71–80 %), 9 (81–90 %), or 10 (91–100 %). Because neoplasm heterogeneity caused variable immunoreactivity in each case, we established a multiplication score for improvement of accuracy: The minimum score was intensity 0×proportion 0 (multiplication score 0), and the maximum was intensity 3×proportion 10 (multiplication score 30). Several representative fields were examined.

Double-staining immunohistochemistry

For double immunostaining, paraffin-embedded tissue sections were deparaffinized in xylene (10 min, two times) and rehydrated through a graded ethanol series. Antigen retrieval was performed by immersing sections in 10 mM Tris-1 mM EDTA buffer (pH 9.0) and boiling in a microwave oven (95 °C, 30 min). After washing of the sections with PBS (5 min, three times), they were allowed to cool at room temperature. They were then incubated in 3 % hydrogen peroxide for 10 min to inactivate endogenous peroxidase. After washing in PBS (5 min, three times), they were incubated with anti-maspin antibody (BD, G167-70, ×50) overnight at 4 °C. The following day, the sections were washed in PBS (5 min, three times), and immunostaining was performed by a standard immunoperoxidase technique (Histofine SAB-PO Kit, Nichirei Co., Tokyo, Japan) with a BCIP/NBT substrate system (Dako Laboratories) as chromogen, according to the manufacturer's instructions. After the sections were washed in distilled water (5 min, three times), antigen retrieval

was performed by immersing the sections in 10 mM Tris-1 mM EDTA buffer (pH 9.0) and boiling in a microwave (95 °C, 10 min). The sections were washed with PBS (5 min, three times) and allowed to cool to room temperature. Subsequently, the sections were incubated with anti-cldn18 antibody (Invitrogen, polyclonal, ×100) overnight at 4 °C. The following day, after the sections were washed in PBS (5 min, three times), immunostaining was performed with the Dako REAL™ EnVision™ Detection System (Dako ChemMate, Glostrup, Denmark) with diaminobenzidine (Dako Laboratories) as the chromogen, according to the manufacturer's instructions. Sections were then counter-stained with hematoxylin, dehydrated, and mounted.

Immunohistochemical analysis of presurgical biopsy specimens

As an additional study, immunohistochemical analysis was performed on 58 samples (18 adenocarcinomas, 21 malignancy-undetermined atypical epithelia, and 19 non-neoplastic lesions) taken from presurgical extrahepatic bile duct forceps biopsies and 7 samples (4 adenocarcinomas and 3 non-neoplastic lesions) taken from presurgical percutaneous biopsies. All specimens of malignancy-undetermined atypical epithelium showed nuclear atypia and turned out to be adenocarcinoma by histological examination of the subsequent surgical specimens. The 19 specimens with non-neoplastic lesions from endobiliary forceps biopsies comprised 5 specimens of IgG4-related sclerosing cholangitis, 5 of primary sclerosing cholangitis, and 9 of nonspecific fibrosis/inflammation. All three specimens of non-neoplastic lesions from percutaneous liver biopsies concerned nonspecific fibrosis/inflammation. None of the patients had a stent when the biopsy was performed. The immunohistochemical protocol was the same as that described above. Because of the small amount of epithelium in biopsy specimens, any immunoreactivity in epithelial cells was regarded as positive regardless of the multiplication score. A case with one or more positive atypical epithelia was given a binary value of 1, while absence of positive atypical epithelia was given a binary value of 0.

Statistics

A three-step analysis was used for the surgical specimens. In the first step, cutoff values were calculated for the multiplication scores of cldn18, maspin (N), and p53 that would distinguish the following: (i) adenocarcinoma from non-neoplastic epithelium, (ii) BilIN from non-neoplastic epithelium, and (iii) neoplasm (adenocarcinoma/BilIN) from non-neoplastic epithelium. In the second step, other cutoff values were calculated for the combined multiplication scores from cldn18, maspin (N), and p53 that would distinguish neoplastic (adenocarcinoma/BilIN) from non-neoplastic epithelium. Third, for every antibody, the multiplication score was converted to its respective binary value using cutoff values obtained in the first step as the threshold. The score with the highest sensitivity and specificity was used to define the receiver operator characteristic (ROC) curve, and the area under the receiver operator characteristic curve (AUC) was calculated. We used 95 % confidence intervals (CIs) to test the hypothesis that AUC is 0.5. For presurgical biopsy specimens, ROC curve analysis was performed to calculate the best binary value in the combination of cldn18, maspin (N), and p53. All statistical analyses were performed with SPSS statistics ver. 20.

Results

Patient characteristics

The study population of 66 patients with biliary tract cancers consisted of 47 men and 19 women, ranging at the time of diagnosis between 39 and 84 years of age (Table 1). The median age of the patients was 68.5 years. The number of patients according to UICC stage was as follows: intrahepatic bile duct cancer I/II n=20 and III/IV n=7, and extrahepatic bile duct and ampullary carcinoma 0/IA/IB/II n=17 and IIA/IIB/III/IV n=22. Cases of BilIN were classified as 8 of BilIN-1, 11 of BilIN-2, and 6 of BilIN-3 as described in the "Materials and methods." None of the patients had papillary lesions identified as IPNB.

Cldn18 expression in surgical specimens

First, we examined the immunochemistry of the surgical specimens for cldn18, maspin, and p53 independently. In the biliary tract tissues, immunostaining of cldn18 was observed in the basolateral membrane of the neoplastic cells (Fig. 1). In contrast, staining for cldn18 was almost absent in non-neoplastic epithelial cells. To maximize reproducibility and accuracy of the immunohistochemical evaluation, we defined a parameter, designated as the multiplication score, which was calculated by multiplying intensity (4 grades) and proportion (11 grades) of immunoreactivity. The multiplication scores for cldn18 in adenocarcinoma, BilIN-3, BilIN-2, BilIN-1, and non-neoplastic epithelium were (mean±SD/median) 22±6.8/24, 26±2.8/27, 25±6.1/27, 23±9.1/27, and 0.97±2.3/0, respectively (Table 2).

In adenocarcinomas, the multiplication score was lower because differentiation of the neoplasm was poor. Multiplication scores in well, moderately, and poorly differentiated adenocarcinoma were (mean±SD/median) 23±5.8/24, 21±8.2/24, and 17±7.5/18, respectively (Table 3

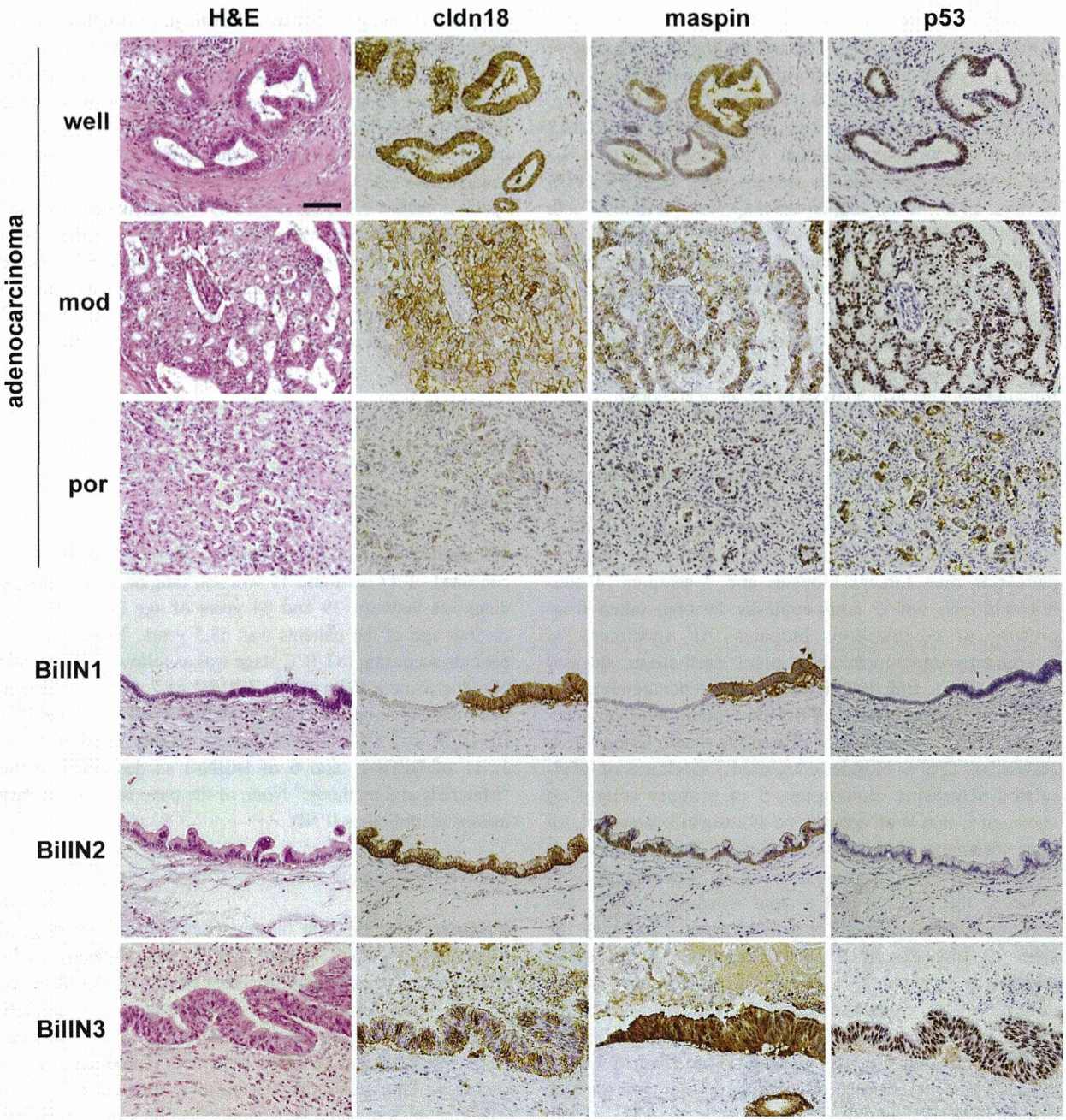

Fig. 1 H&E staining and immunohistochemical staining in surgical specimens of well, moderately (mod), and poorly (por) differentiated bile duct adenocarcinoma and BilIN-1, BilIN-2, and BilIN-3. Cldn18 was expressed on basolateral membranes of the epithelial cells in adenocarcinoma and BilIN-1, BilIN-2, and BilIN-3. Maspin was also expressed in both the cytoplasm and nucleus of the epithelial cells in adenocarcinoma and BilIN-1, BilIN-2, and BilIN-3. p53 was expressed in the nucleus of the epithelial cells in some specimens of adenocarcinoma and BilIN-2 and BilIN-3. In the non-neoplastic epithelial cells adjacent to BilIN, none of the three antibodies caused staining

and Supplementary Fig. S1). Cldn18 was distributed along the entire cell membrane of most cells in well-differentiated adenocarcinomas and expressed at least in part on the cell surfaces of poorly differentiated adenocarcinoma cells (Fig. 1). There were no significant changes in the cldn18 expression patterns in BilIN-1, BilIN-2, and BilIN-3.

Maspin expression in surgical specimens

Immunostaining of maspin was observed in both the cytoplasm and nucleus of the neoplastic cells (Fig. 1). Apart from bile duct epithelium, some non-neoplastic hepatic cells and duodenal epithelial cells were positive

Table 2 Results of the immunohistochemical evaluation of cldn18, maspin, and p53 in surgical specimens

			Intensity		Proportion		Multiplication score	
Antibody	Histological type	Number	Mean±SD	Median	Mean±SD	Median	Mean±SD	Median
cldn18	Adenocarcinoma	66	2.8±0.5	3	7.7±1.9	8	22±6.8	24
	BilIN-3	6	3±0	3	8.7±1.0	9	26±2.8	27
	BilIN-2	11	3±0	3	8.3±2.0	9	25±6.1	27
	BilIN-1	8	2.6±0.70	3	8.1±2.1	9	23±9.1	27
	Non-ne	63	0.48±0.73	0	0.73±1.6	0	0.97±2.3	0
Maspin (C)	Adenocarcinoma	66	2.3±1.2	3	5.0±3.2	5.5	14±9.7	15
	BilIN-3	6	2.7±0.5	3	6.2±2.9	6	17±9.5	15
	BilIN-2	11	2.3±1.1	3	5.0±3.7	5	15±11	15
	BilIN-1	8	1.6±1.3	2	2.6±2.8	2	7.3±8.6	4
	Non-ne	63	0.35±0.91	0	0.33±0.85	0	0.79±2.1	0
Maspin (N)	Adenocarcinoma	66	2.5±1.0	3	5.1±3.0	6	15. ± 9.4	18
	BilIN-3	6	3.0±0	3	5.7±1.6	6.5	17±4.8	19.5
	BilIN-2	11	2.0±1.3	3	4.5±3.6	5	13±11	15
	BilIN-1	8	1.9±1.3	2.5	3.8±3.0	3	10±9.6	6
	Non-ne	63	0.57±1.1	0	0.57±1.1	0	1.5±3.0	0
p53	Adenocarcinoma	66	1.7±1.3	2	2.7±3.1	1	7.4±9.5	3
	BilIN-3	6	1.2±1.1	1	2.2±2.4	1	4.3±6.3	1.5
	BilIN-2	11	0.64±1.1	0	0.73±1.7	0	2±5.1	0
	BilIN-1	8	0.63±1.1	0	1±2.3	0	2.9±6.9	0
	Non-ne	63	0	0	0	0	0	0

Non-ne non-neoplastic epithelium

for maspin in the nucleus. Multiplication scores for maspin (C) in adenocarcinoma, BilIN-3, BilIN-2, BilIN-1, and non-neoplastic epithelium were (mean±SD/median) 14±9.7/15, 17±9.5/15, 15±11/15, 7.3±8.6/4, and 0.79±2.1/0, respectively (Table 2). Multiplication scores for maspin (N) in adenocarcinoma, BilIN-3, BilIN-2, BilIN-1, and non-neoplastic epithelium were (mean±SD/median) 15±9.4/18, 17±4.8/19.5, 13±11/15, 10±9.6/6, and 1.5±3.0/6, respectively (Table 2). Multiplication scores for maspin (N) in well, moderately, and poorly differentiated adenocarcinoma were (mean±SD/median) 17±8.2/21, 12±10/10.5, and 14±9.9/12, respectively (Table 3 and Supplementary Fig. S1). There were no significant differences

Table 3 Results of the immunohistochemical evaluation of well, moderately, and poorly differentiated adenocarcinoma in surgical specimens

			Intensity		Proportion		Multiplication score	
Antibody	Differentiation	Number	Mean±SD	Median	Mean±SD	Median	Mean±SD	Median
cldn18	Well	33	2.9±0.4	3	8.0±1.5	8	23±5.8	24
	Moderately	16	2.7±0.7	3	7.8±2.2	8	21±8.2	24
	Poorly	17	2.2±0.7	2	7.2±2.1	8	17±7.5	18
Maspin (C)	Well	33	2.5±1.0	3	5.9±3.0	7	17±9.5	21
	Moderately	16	1.9±1.2	2.5	4.1±3.1	4	10±9.2	8.5
	Poorly	17	2±1.3	3	4±3.1	4	11±9.2	12
Maspin (N)	Well	33	2.6±0.8	3	5.8±2.6	7	17±8.2	21
	Moderately	16	2.1±1.3	3	4.1±3.4	3.5	12±10	10.5
	Poorly	17	2.4±1.0	3	4.8±3.2	5	14±9.9	12
p53	Well	33	1.8±1.3	2	2.9±3.2	1	7.8±9.6	3
	Moderately	16	1.6±1.2	2	2.9±3.2	1	7.5±9.3	2.5
	Poorly	17	1.6±1.3	2	2.1±2.8	1	5.8±8.7	2

in the scores among adenocarcinomas (all histological types; data not shown).

p53 expression in surgical specimens

p53 was expressed in the nucleus in some adenocarcinomas and a few specimens with BilIN-2 and BilIN-3 (Fig. 1). Multiplication scores in specimens with adenocarcinoma, BilIN-3, BilIN-2, BilIN-1, and non-neoplastic epithelium were (mean±SD/median) 7.4±9.5/3, 4.3±6.3/1.5, 2.0±5.1/0, 2.9±6.9/0, and 0/0, respectively (Table 2). For each neoplasm, the multiplication scores for p53 were lower than those for cldn18 and maspin, but p53 was the most specific of the three markers (Table 2). Multiplication scores in well, moderately, and poorly differentiated adenocarcinoma were (mean±SD/median) 7.8±9.6/3, 7.5±9.3/2.5, and 5.8±8.7/2, respectively (Table 3 and Supplementary Fig. S1).

Diagnostic value of cldn18, maspin, and p53 in surgical specimens

To distinguish neoplasms from non-neoplastic epithelium in the surgical specimens from patients with biliary tract cancers, we calculated the AUC for cldn18, maspin, and p53, as described in the "Materials and methods" (Fig. 2a). The AUC for cldn18 was 0.992 [95 % CI, 98.3 to 100] (Fig. 2b). A cutoff value of 6 produced the highest accuracy (minimal number of false-negative and false-positive results); sensitivity and specificity were 95.6 and 96.8 %, respectively. There was no significant difference in the scores between BilIN-1–3, so BilIN-1–3 were referred to collectively as "BilIN" (Fig. 2c). As shown in the upper panel of Fig. 2c, 87 of 91 (95.1 %) specimens with adenocarcinoma/BilIN (63 of 66 with adenocarcinoma and 24 of 25 with BilIN) were detected as neoplastic. Among specimens with non-neoplastic epithelium, 61 of 63 (96.8 %) were detected as non-neoplastic. The AUC for maspin (N) was 0.879 [95 % CI, 82.5 to 93.3] (Fig. 2b). A cutoff value of 1 gave the highest accuracy; sensitivity and specificity were 85.6 and 77.8 %, respectively. As shown in the third panel of Fig. 2c, 78 of 91 (85.7 %) specimens with adenocarcinoma/BilIN (58 of 66 with adenocarcinoma and 20 of 25 with BilIN) were detected as neoplastic. Among the specimens with non-neoplastic epithelium, 49 of 63 (77.8 %) were detected as non-neoplastic. The AUC for p53 was 0.806 [95 % CI, 73.7 to 87.4] (Fig. 2b). A cutoff value of 1 produced the highest accuracy; sensitivity and specificity were 61.1 and 100 %, respectively. As shown in the bottom panel of Fig. 2c, 56 of 91 (61.5 %) specimens with adenocarcinoma/BilIN (47 of 66 with adenocarcinoma and 9 of 25 with BilIN) were detected as neoplastic. Among specimens with non-neoplastic epithelium, all 63 were detected as non-neoplastic. For distinguishing adenocarcinoma from non-neoplastic epithelium or BilIN from non-neoplastic epithelium, ROC curves showed that all the three markers were highly accurate (Supplementary Figs. S2A and S2B).

Next, we obtained additional scores by combining the multiplication scores for cldn18, maspin (N), and p53 and analyzed the new scores to distinguish neoplastic from non-neoplastic tissues. The AUC for the combined multiplication score was 0.996 [95 % CI, 98.8 to 100] (Supplementary Fig. S3A). A cutoff value of 15 had the highest specificity; sensitivity and specificity were 96.6 and 100 %, respectively. A cutoff value of 12 had the highest sensitivity; sensitivity and specificity were 100 and 96.8 %, respectively (Supplementary Fig. S3A). When all specimens were differentiated by a cutoff value of 15, 88 of 91 (96.7 %) specimens with adenocarcinoma/BilIN were detected as neoplastic, and all 63 specimens with histologically diagnosed non-neoplastic epithelium were detected as non-neoplastic (Supplementary Fig. S3B). These results indicate that the strategy of combining the three multiplication scores successfully distinguished neoplasms from non-neoplastic epithelia in the surgical specimens of biliary tract carcinoma.

For convenience, we employed an additional step. Before combining the three parameters for cldn18, maspin (N), and p53, we converted each of the multiplication scores to binary values (0 for immuno-negative and 1 for immuno-positive) on the basis of the best cutoff values calculated above. With the binary values for cldn18, maspin (N), and p53, we calculated the AUC and analyzed the new scores to distinguish neoplasms from non-neoplastic tissues (Fig. 3). After these processes, the AUC was 0.989 [95 % CI, 97.8 to 99.9] (Fig. 3a). As shown in Fig. 3b, the best cutoff score was 2, 81 of 91 (89.0 %) specimens with adenocarcinoma/BilIN and none with non-neoplastic epithelium were distinguished as neoplastic, and sensitivity and specificity were 91.1 and 100 %, respectively. At a cutoff value of 1, all 91 specimens with adenocarcinoma/BilIN and 15 of 63 (23.8 %) with non-neoplastic epithelium were distinguished as neoplastic; sensitivity and specificity were 100 and 74.6 %, respectively. At a cutoff value of 3, 41 of 91 (45.1 %) specimens with adenocarcinoma/BilIN and none with non-neoplastic epithelium were distinguished as neoplastic; sensitivity and specificity were 51.1 and 100 %, respectively.

Diagnostic value of cldn18, maspin, and p53 in presurgical endobiliary forceps biopsy specimens

Next, we examined whether this analysis is applicable to presurgical endobiliary forceps biopsy specimens because they are the most important source for both clinical diagnosis and rapid intraoperative diagnosis. The immunostaining patterns of the presurgical endobiliary forceps biopsy specimens were similar to those of the surgical specimens (Fig. 4a). In biopsy specimens, we observed that some epithelia without apparent dysplasia, including intestinal epithelium, were

a

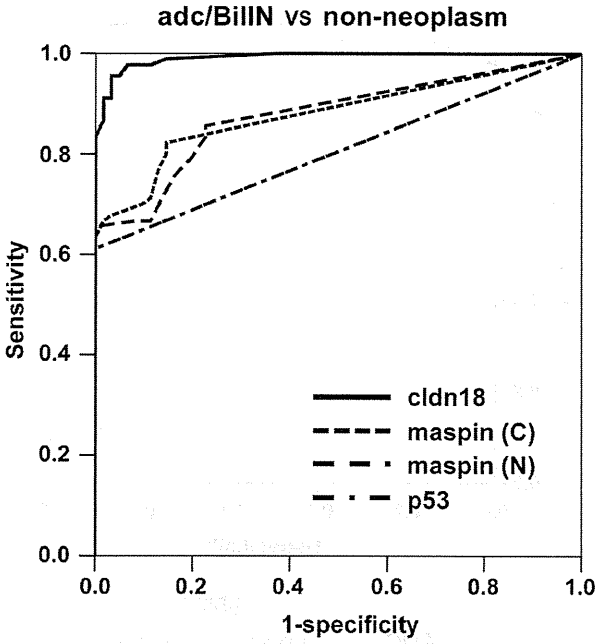

b

		95%CI	
	AUC	Lower	Upper
cldn18	0.992	0.983	1.000
maspin (C)	0.881	0.826	0.935
maspin (N)	0.879	0.825	0.933
p53	0.806	0.737	0.874

score	Best cutoff	Sensitivity	Specificity
cldn18	≥6	0.956	0.968
maspin (C)	≥1	0.822	0.857
maspin (N)	≥1	0.856	0.778
p53	≥1	0.611	1.000

c